

**200 and 300 MeV/nucleon nuclear reactions responsible for single-event effects in microelectronics**

H. Jäderström,<sup>1,\*</sup> Yu. Murin,<sup>2,3</sup> Yu. Babain,<sup>2</sup> M. Chubarov,<sup>2</sup> V. Pljushev,<sup>2</sup> M. Zubkov,<sup>2</sup> P. Nomokonov,<sup>3</sup> N. Olsson,<sup>4</sup> J. Blomgren,<sup>5</sup> U. Tippawan,<sup>5</sup> L. Westerberg,<sup>6</sup> P. Golubev,<sup>7</sup> B. Jakobsson,<sup>7</sup> L. Gerén,<sup>8</sup> P.-E. Tegnér,<sup>8</sup> I. Zartova,<sup>8</sup> A. Budzanowski,<sup>9</sup> B. Czech,<sup>9</sup> I. Skwirczynska,<sup>9</sup> V. Kondratiev,<sup>10</sup> H. H. K. Tang,<sup>11</sup> J. Aichelin,<sup>12</sup> Y. Watanabe,<sup>13</sup> and K. K. Gudima<sup>14</sup>

<sup>1</sup>*Department of Nuclear and Particle Physics, Uppsala University, Box 531, S-751 21 Uppsala, Sweden*

<sup>2</sup>*V. G. Khlopin Radium Institute, 2nd Murinski prospect 28, RU-194021 Saint-Petersburg, Russia*

<sup>3</sup>*Joint Institute for Nuclear Research, JINR, RU-141980, Dubna, Russia*

<sup>4</sup>*Swedish Defence Research Agency (FOI), S-172 90 Stockholm, Sweden*

<sup>5</sup>*Department of Neutron Research, Uppsala University, Box 525, S-751 20 Uppsala, Sweden*

<sup>6</sup>*Department of Physics, Uppsala University, Box 530, S-751 21 Uppsala, Sweden*

<sup>7</sup>*Department of Physics, Lund University, Box 118, S-221 00 Lund, Sweden*

<sup>8</sup>*Department of Physics, Stockholm University, S-10691 Stockholm, Sweden*

<sup>9</sup>*H. Niewodniczanski Institute of Nuclear Physics, 31-342 Cracow, Poland*

<sup>10</sup>*St. Petersburg State University, RU-198504 St. Petersburg, Russia*

<sup>11</sup>*IBM, T. J. Watson Research Center, Yorktown Heights, New York 10598, USA*

<sup>12</sup>*IN2P3/CNRS, Ecole des Mines de Nantes, 4 rue Alfred Kastler, F-44072 Nantes cedex 03, France*

<sup>13</sup>*Department of Advanced Energy Engineering Science, Kyushu University, Kasuga, Fukuoka 816-8580, Japan*

<sup>14</sup>*Institute of Applied Physics, Moldova Academy of Sciences, MD-2028 Kishinev, Moldova*

(Received 27 November 2007; published 7 April 2008)

An experimental study of nuclear reactions between  $^{28}\text{Si}$  nuclei at 200 and 300 MeV/nucleon and hydrogen or deuterium target nuclei was performed at the CELSIUS storage ring in Uppsala, Sweden, to collect information about the reactions responsible for single-event effects in microelectronics. Inclusive data on  $^{28}\text{Si}$  fragmentation, as well as data on correlations between recoils and spectator protons or  $\alpha$  particles are compared to predictions from the Dubna cascade model and the Japan Atomic Energy Research Institute version of the quantum molecular dynamics model. The comparison shows satisfactory agreement for inclusive data except for He fragments where low-energy sub-barrier fragments and recoiling fragments with very large momenta are produced much more frequently than predicted. The yield of exclusive data are also severely underestimated by the models whereas the charge distributions of recoils in these correlations compare well. The observed enhancement in He emission, which may well be important for the description of single-event effects, is most likely to be attributed to  $\alpha$  clustering in  $^{28}\text{Si}$  nuclei.

DOI: [10.1103/PhysRevC.77.044601](https://doi.org/10.1103/PhysRevC.77.044601)

PACS number(s): 25.40.Sc, 25.45.-z, 27.30.+t, 34.50.Bw

## I. INTRODUCTION

In this article we present the results of an experimental study of  $^{28}\text{Si}+^1\text{H}$  and  $^{28}\text{Si}+^2\text{H}$  reactions at 200 and 300 MeV/nucleon in inverse kinematics. The experiments were carried out at the CELSIUS storage ring of The Svedberg Laboratory, Uppsala, Sweden. The aim was twofold: to measure useful cross sections for the description of the single-event effects (SEEs) reactions and to describe such reactions with up-to-date models for  $p$ -nucleus collisions. The most prominent of all SEEs, the single-event upset (SEU) effect is manifested by the functional upsets of microelectronic memory devices primarily in space missions but also in aviation and even, to a lesser extent, at sea level [1,2].

Nuclear fragmentation of light nuclei induced by cosmic rays is related to the SEEs and other important applications, like optimizing microdosimetry for human tissue in radiation therapy. Theoretical “toolkits” have been developed but they are based on standard reaction models for heavy nuclei and

may wash out important details in the topology of light nucleus fragmentation. The strong  $\alpha$  clustering that we report on in this work may in fact be evidence for nuclear structure effects that are ignored in (multi-)fragmentation models. Another complication arises from the fact that in the energy domain of 50–500 MeV/nucleon, most interesting for the applications, the basic assumptions of the models are not valid. These energies are well above the Coulomb barrier but not high enough to assure that the quasi-classical approximation is fully satisfied or that all quantum effects can be neglected.

Theoretical models for intermediate energy  $p$ -nucleus and nucleus-nucleus collisions have been developed over the past four decades [3–5]. The uncertainties in the models and the lack of detailed experimental data motivated this experiment. At low altitudes the source of nuclear reactions producing upsets in chips made of Si is the neutron component of atmospheric cosmic rays. These neutrons have a broad energy range [6] that spreads from about 50 to 1000 MeV. The  $n+\text{Si}$  reaction is difficult to study and therefore measurements of the inverse kinematics,  $^{28}\text{Si}+^1\text{H}$ ,  $^2\text{H}$  reactions are investigated in this work. In fact it is believed that the recoils, i.e., reaction products with charge  $2 < Z \leq 14$ , are to a large degree

\*henrik.jaderstrom@tsl.uu.se

responsible for SEEs and therefore comprehensive data on light nucleus fragmentation at medium energy in general is important to collect. Typical ranges for these recoils are only a few microns in the detector. This is the major reason why there are so few recoil measurements. After pioneering work [7] on light ion production in  $p$ -nucleus reactions, one single experiment [8], bombarding 180-MeV protons on aluminum, reports on recoil production. The results of Ref. [9] are rather a good example of the crucial limitations in experiments on spallation of light target nuclei in normal kinematics. The basic idea of this project was to study fragmentation of silicon nuclei induced by medium-energy protons in the inverse kinematics scheme that gives much more favorable conditions to measure the heavy recoils with standard techniques [8–10].

Because it was not expected that one single model is able to describe the detailed data from this experiment, we choose to compare it with two well-known microscopic descriptions, the intranuclear cascade (INC) model and the quantum molecular dynamics (QMD) model. The mathematical formulation offered by the Dubna cascade model (DCM) [3,4] was utilized for the INC calculations. For calculations within the QMD framework, we used the model developed at the Japan Atomic Energy Research Institute (JAERI) in Japan (JQMD) [5]. DCM and JQMD are briefly described below. Both models are well known and have been reported to yield successful comparisons with experimental data on inclusive production of light particles ( $n$ ,  $p$ , He) in hadron-nucleus and nucleus-nucleus collisions at intermediate energies [11], as well as at energies of several GeV. Both models are widely used for various practical applications [12–18]. The two approaches differ in their view of the recoils, where INC interprets them as the remnants of a long chain of individual emission of light nuclei from the highly excited source, whereas QMD generates recoils instantly through the cracking of an almost cold initial source with subsequent evaporative emission of light particles.

It is not at all obvious a priori that significant discrepancies between the recoil distributions from the two models should appear, especially because evaporation tends to smear out possible, initial differences. We will come back to this question in Sec. IV.

## II. THE LAYOUT OF THE EXPERIMENT

The experiment was carried out at the cluster-jet target and the following quadrant of the CELSIUS ring. The experimental setup has been described in detail in Ref. [19] and only a brief description is given below. The layout of the experiment is shown in Fig. 1. The luminosity in the  $^{28}\text{Si}+^1\text{H}$  reaction with an accelerated and cooled beam interacting with the hydrogen jet target was  $\sim 5 \times 10^{27} \text{ cm}^{-2} \text{ s}^{-1}$ .

Secondary particles were registered simultaneously by four detector systems, the small angle detector (SAD), the forward wall detector (FWD), the zero angle detector (ZAD), and the spectator tagging detector (STD). FWD and STD (CHICSi) had been used in previous experiments at CELSIUS and are described elsewhere [20–25]. SAD and ZAD play a key role because they detect the product recoils, which are most important for the SEEs.

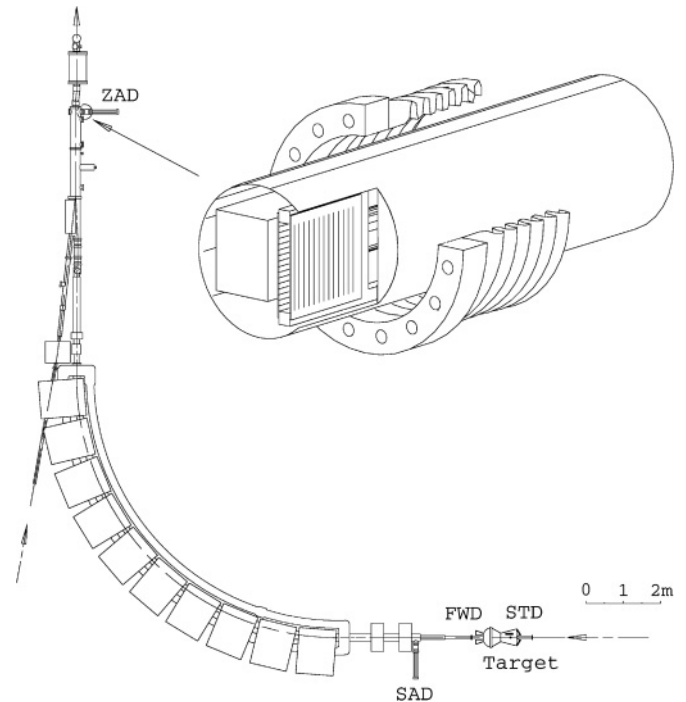


FIG. 1. Overview of the experimental setup.

SAD detects fragments from the  $^{28}\text{Si}$  beam nuclei emitted at angles  $0.6^\circ$ – $1.1^\circ$ . It consists of two quadrants with 16 circular and 16 radial  $300\text{-}\mu\text{m}$  Si strip detectors in front of an 8-mm plastic scintillator. Here, the unique properties of the cooled beam are fully exploited. During the injection and acceleration phases of the cycle, the beam occupies a large volume of the CELSIUS vacuum chamber but after the beam has been cooled, it shrinks to a diameter of 2 mm. To prevent the SAD detectors from radiation damage, they were moved out during injection/acceleration and returned to working position only after the beam reached maximum energy. The design of SAD is described in Ref. [19].

FWD [20] was used mainly for detection of light ( $A \leq 4$ ) fragments emitted in the  $3.9^\circ$ – $11.7^\circ$  angular bin. In this experiment it consisted of twenty-four  $750\text{-}\mu\text{m}$  Si detectors followed by 1-mm fast plastic scintillators glued on top of 80-mm-long CsI crystals. The main task for the FWD was to register He fragments in coincidence with recoils registered by SAD.

One Grand Motherboard (GMB) of the CHICSi detector [21–23] with 12 Si and 6 Si+GSO  $\Delta E$ - $\Delta E$ -E telescopes mounted inside the ultrahigh vacuum chamber was used to tag events by spectator particles. Protons from the angular region  $60^\circ$ – $120^\circ$  identified as knocked-out free protons in the  $^{28}\text{Si}+^1\text{H}$  and bound protons in the  $^{28}\text{Si}+^2\text{H}$  reaction allowed us to extract Si+ $n$  data that represent the dominating source of SEEs in the atmosphere.

The ZAD is a telescope comprising two SSDs and a plastic scintillator similar to the one used in SAD. Here we make use of a technique developed at TSL [24,25] where the CELSIUS quadrant after the cluster-jet target is used as a magnetic spectrometer. ZAD is positioned at the focal plane of the spectrometer at a 22757-mm flight distance from the target.

In ZAD the strips make up a  $32 \times 32$  rectangular net with a  $60 \times 60 \text{ mm}^2$  area. Vertical and horizontal strips of SSDs are used to detect projectile fragments, identify their charge, and determine the position of the hit point with respect to the nominal beam centerline. The electronic schemes of SAD and ZAD are identical [19].

At high recoil energy in the laboratory system the efficiency of the detectors approaches 100%. However, with the absence of detectors in the angular interval  $1.1^\circ$ – $3.9^\circ$  a significant fraction of the recoils, and especially the lighter ones, are not detected, which makes it impossible to measure the total cross sections directly.

### III. THEORETICAL TOOLS

The basic idea of Serber [26], formulated in 1947, that  $p$ -nucleus (and heavy-ion) reactions at energies above 150 MeV/nucleon could be described as a superposition of binary nucleon-nucleon collisions, well separated in time and space, is still a common starting point for all models. The motivation for such a view is that the de Broglie wavelength of the bombarding nucleon(s) is getting smaller than the average intra nucleon distance. All INC models contain nucleon-nucleon collision chains as a first stage of the reaction, during which fast nucleons are ejected from the heavy nucleus. The INC is a rapid process that develops fully in approximately  $10^{-22}$  s. It must, however, be supplemented with a statistical “after-burner” to describe the large yields of low-energy nucleons and light fragments observed in the experiments. Often evaporation from the excited remnants is introduced and this is a relatively slow process ( $10^{-21}$ – $10^{-17}$  s) and it can therefore be regarded as the second stage of the reaction. The recoils are then considered as the “leftovers” of the two-stage process. Even if Serber’s assumption is strictly not valid for collisions at lower energies, INC models have been reported to work well also for proton-induced reactions at energies as low as 60 MeV [15].

Several attempts to generalize the cascade-evaporation description have been made. Pre-equilibrium emission of particles between the first and the second stage of the reaction has been described within the Harp-Miller-Berne model [27], the Griffin exciton model [28], and its various later versions [29]. The Feshbach-Kerman-Koonin theory [30] was the first attempt to introduce quantum mechanics in the description of reactions at reasonably low energies. All these approaches have in fact mostly been used to describe low-energy reactions (20–150) MeV but even at much higher energies they do contain all necessary ingredients important for the description of the rescattered moderate-energy nucleons within the cascade. The modern INC models are in fact essentially based on the same ideas for building a three-stage sequence, i.e., INC, pre-equilibrium, and equilibrium evaporation as the driving mechanism of nuclear fragmentation.

QMD models appeared two decades ago to describe nuclear reactions. They consider the equations-of-motion of the nucleons in a concept borrowed from molecular physics. The molecular and nuclear versions differ in their most general formulation due to the difference of space and time scales.

Nevertheless, in both cases QMD is the method to numerically solve the time-dependent Schrödinger equations for nucleons moving in a realistic potential and with a collision term similar to that used in transport theory [31]. A strong feature of the QMD approach is its natural inclusion of dynamics, which allows studies of collisions of large systems in real time.

QMD was first used for medium energy nucleus-nucleus collisions [32] and immediately a whole set of models [33,34] was developed to exploit the QMD method for all kinds of reactions. Often assumptions and parameters are borrowed in these models from the INC model to such an extent that final results from the models of the two types discussed also come out similarly and it is difficult to refine the differences between the two conceptually different theoretical approaches. In this work we confronted our experimental data with versions of the two models, each representing the two different approaches to the problem. Microscopic calculations have been performed within the time-dependent version of the Dubna intranuclear cascade model (DCM) (see Refs. [3,4] and references therein). The QMD model that we use, JQMD, has been developed at JAERI in Japan [5].

DCM divides the collision into three stages, well separated in time. During the first initial stage INC develops, primary particles can scatter and secondary particles can re-scatter several times prior to their absorption or escape from the nucleus. At the end of this step the coalescence model is used to localize  $d$ ,  $t$ ,  $^3\text{He}$ , and  $^4\text{He}$  particles from nucleons found inside spheres with well-defined radii in configuration space and momentum space. The emission of cascade particles determines a particle-hole configuration, i.e.,  $Z$ ,  $A$ , and excitation energy that is taken as the starting point for the second, pre-equilibrium stage of the reaction, described according to the standard Gudima-Toneev prescription, CEM [3] in its latest version CEM03.01 [35]. Some pre-equilibrium particles may be emitted and this leads to a lower excitation of the thermalized residual nuclei. In the third, final evaporation/fission stage of the reaction, the de-excitation of the residue is described with the generalized evaporation model (GEM) of Furihata [36]. All components contribute normally to the final spectra of particles and light fragments. If, however, the residual nuclei after the INC have atomic numbers  $A < 12$ , the Fermi breakup model [37] is used instead to describe their further disintegration instead of GEM. For relativistic energies the INC part of DCM is replaced by the refined cascade model, which is a version of the quark-gluon string model (QGSM) developed in Ref. [38] and extended to intermediate energies in Ref. [39].

The description of the mean-field evolution is simplified in the DCM in the sense that the scalar nuclear potential, defined by the local Thomas-Fermi approximation, remains the same throughout the collision. Only the potential depth changes in time according to the number of knocked-out nucleons. This “frozen mean-field” approximation allows us to take into account the nuclear binding energies and the Pauli exclusion principle, as well as to estimate the excitation energy of the residual nucleus by counting the excited particle-hole states (excitons). This approximation is usually considered to work particularly well for hadron-nucleus collisions.

The well-documented JQMD code in its standard version [5] is our second choice of model. This is also a hybrid

model with a first QMD step and the statistical decay model (SDM) [40] as second step. This code introduces relativistic kinematics and relativistic corrections for the interaction term, the Lorentz boost of the initial and final states, realistic momentum distributions in the ground state, and a comprehensive nucleon-nucleon collision term [5]. The model works well for pre-equilibrium emission of particles in proton induced collisions [4,5]. In medium-energy nucleus-nucleus collisions [41] the emission of light fragments requires some minor refinements in the code. For reactions close to those studied in this work, JQMD successfully describes fragment production in  $p+^{56}\text{Fe}$  and  $^{27}\text{Al}$  [42] in a wide energy range, from 50 MeV to 5 GeV. It could also be mentioned that JQMD has recently been used for generating a nuclear database on neutron-induced fragmentation of Si [43].

#### IV. EXPERIMENTAL RESULTS CONFRONTED WITH DCM AND JQMD MODELS

In this experiment the charge ( $Z$ ), azimuthal ( $\phi$ ), and polar ( $\theta$ ) angles of the recoils were measured, whereas no energy was determined because the detector systems did not stop the recoils. By calculating the flight trajectories in the magnetic field of the CELSIUS fourth quadrant from the collision point to ZAD [19], the momenta could be obtained for  $0^\circ$  recoils with  $A/Z = 2$ . Whereas all recoils with  $Z \geq 6$  registered in SAD provide good statistics, only a small number of heavier fragments was observed and measured by the FWD. This allows only the determination of inclusive production rates for FWD recoils, whereas recoil-He correlations can be exploited.

The technique to use inverse kinematics reactions in storage rings has the advantages of high luminosity, reduced background, etc., but leads to difficulty in measuring absolute cross sections. Because we used Monte Carlo simulations with complete experimental filters, we chose to normalize the experimental data on He fragments registered in the first ring of FWD at an angle of  $4.9^\circ$  by the corresponding predictions of the DCM model. Table I shows the value of differential cross section used for the normalization. This is justified, first because DCM is quite well established for the emission of He with energies 5–40 MeV and angles  $30^\circ$ – $160^\circ$ , corresponding to the region of phase space explored with FWD when the kinematics are reversed. Second, such an approach provides high statistics for He fragments in FWD and this minimizes the statistical uncertainties of the procedure. The results of the JQMD calculations were taken as they came out but they were not used for the normalization of the experimental

TABLE I. The differential cross section for He at  $4.9^\circ$  used for the normalization.

Reaction	Energy (MeV/nucleon)	$\frac{d\sigma}{d\Omega}$ (b/sr)
$^{28}\text{Si}+^1\text{H}$	200	2.9
$^{28}\text{Si}+^1\text{H}$	300	2.3
$^{28}\text{Si}+^2\text{H}$	200	5.9
$^{28}\text{Si}+^2\text{H}$	300	4.9

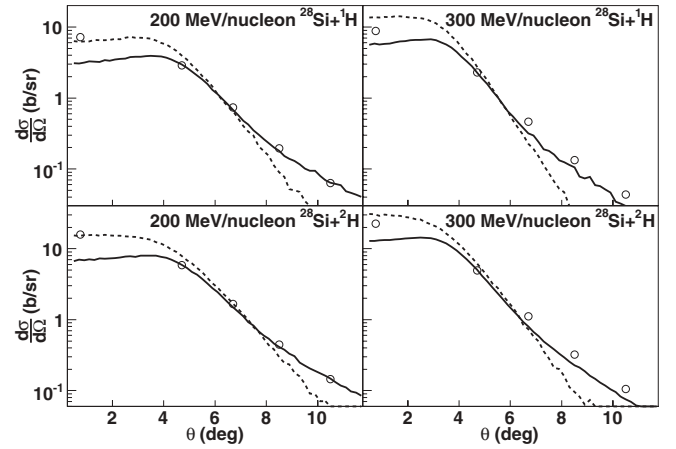


FIG. 2. Angular distribution of He fragments observed with FWD and SAD (open points) for 200 and 300 MeV/nucleon  $^{28}\text{Si}+^1\text{H}$ ( $^2\text{H}$ ) reactions confronted to the prescription of DCM (solid curves) and JQMD (dashed curves). Statistical error bars fall within the point size.

data. DCM shows a better agreement of the shape of the angular distribution in Fig. 2 that justifies the choice of DCM for normalization. We estimate the accuracy of the absolute normalization of the experimental data to be within 20–25% [19].

#### A. Inclusive production of $\alpha$ particles and recoils

Figure 2 shows the angular distributions of He nuclei registered by SAD, the very first point, and by FWD with four points corresponding to polar angles of the four FWD rings. DCM reproduces the shape of the angular distributions for all reactions in the region of FWD but fails quite severely to predict the yield in SAD. The JQMD version of Ref. [5], however, does not reproduce the overall shape of the distributions at all until the improvements, discussed below, are introduced.

Two improvements of the standard JQMD version have been proposed [44,45]. The first one introduces GEM [36] instead of SDM as the evaporation stage. This allows evaporation of heavy fragments. The second improvement is connected with the assumption of coalescence of light particles on the surface of the excited nucleus. This was first introduced to explain the high-energy part of the He particles measured in Ref. [46]. Introducing these two improvements may very well improve the agreement in Fig. 2 for JQMD. However, it is important to remember that the QMD approach meets principal difficulties in describing  $\alpha$  particles [47] due to their specific properties. With this in mind, the better agreement between JQMD and the experimental values for He registered by SAD in Fig. 2 could be accidental and therefore should be taken with caution.

The systematic failure of DCM to describe the production of He nuclei within the SAD angular region is unexpected. These He fragments are almost at rest in the frame of the fragmenting source, which may be the reason why they have never been measured before in conventional experiments with stationary



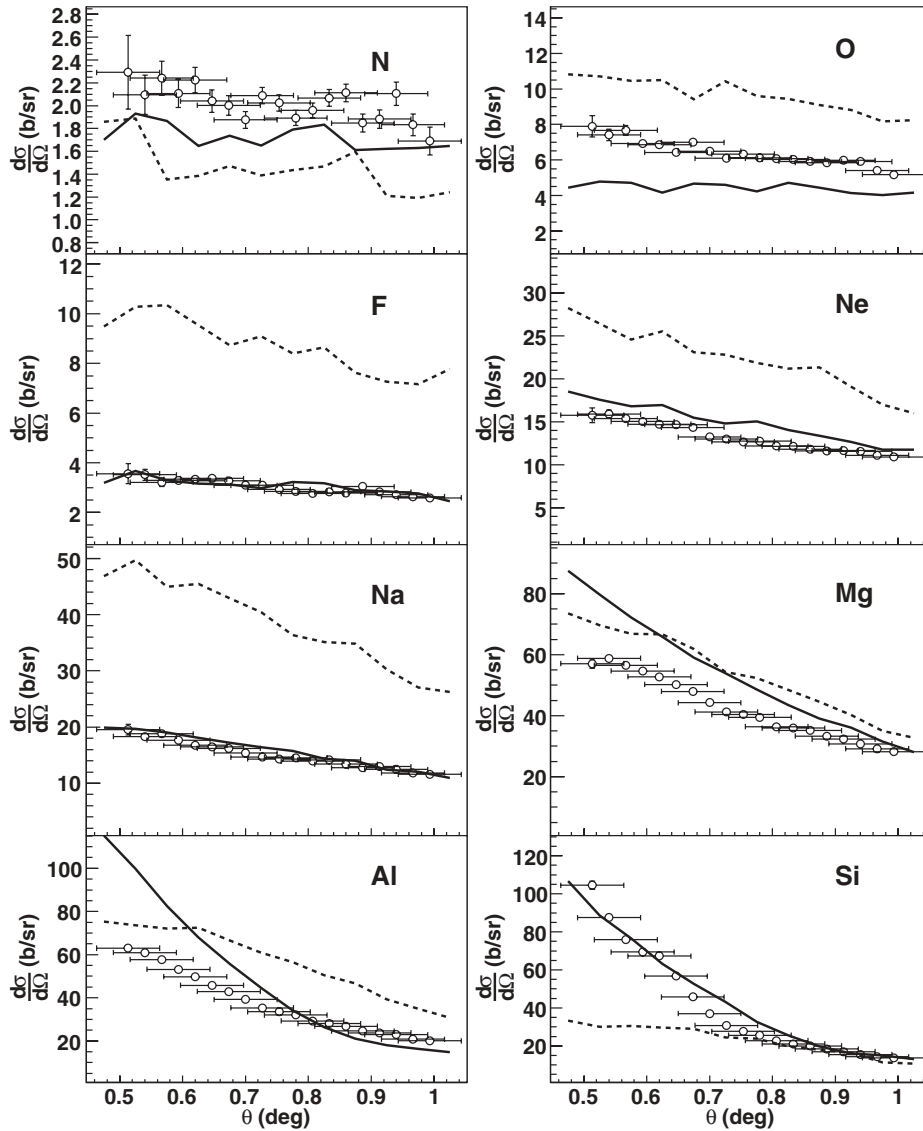


FIG. 3. Angular distribution of recoils in 200 MeV/nucleon  $^{28}\text{Si}+^1\text{H}$  reactions (open points) compared with predictions of DCM (solid curves) and JQMD (dashed curves).

targets. Here, we demonstrate that there is an additional process that is strongly populating the very edge of the phase space of the statistical after-burner. Quasi-elastic scattering of  $\alpha$  clusters preformed in the  $^{28}\text{Si}$  nucleus could be the origin of the observed deviation from theory.

The DCM model was originally constructed for the interpretation of inclusive production of light particles and it was consequently tuned mostly by data of this kind. Therefore, it is especially interesting to check the consistency of this model for both light and heavy fragment production, measured in the same experiment. Figures 3 and 4 show the angular distributions of all recoils for  $^{28}\text{Si}+^1\text{H}$  reactions at 200 and 300 MeV/nucleon. The corresponding angular distributions of recoils in  $^{28}\text{Si}+^2\text{H}$  reactions, not shown for brevity, are very similar.

The experimental data are again shown together with the results of computer simulations based on the prescriptions of DCM (solid curves) and JQMD (dashed curves). Both models predict the general trend in the evolution of the shape with recoil charge rather well. These distributions are

quite broad and structureless. The general tendencies to have broader distributions with decreasing fragment charge and with increasing beam energy are noticeable. Such behavior is qualitatively understood by simple phase-space arguments. The increase of the number of nucleons that are not tied up in the recoil opens up the available phase space of the recoil and so does the increased energy of the beam nucleus.

Yet, it appears from Figs. 3 and 4 that the predicting power of both models is limited to the qualitative angular dependences. The proper absolute levels are achieved only for few fragments without systematic trends. In general the DCM depicts a slightly better predictive power than JQMD for the shape of the angular distributions of the heaviest recoils. The absolute values of cross sections for production of lighter fragments, i.e., O, F, and Na, seem to be grossly overestimated by the JQMD, even if one takes into account the above mentioned uncertainties in absolute normalization of the data.

As mentioned above the experimental information on production of recoils from medium-energy reactions with light

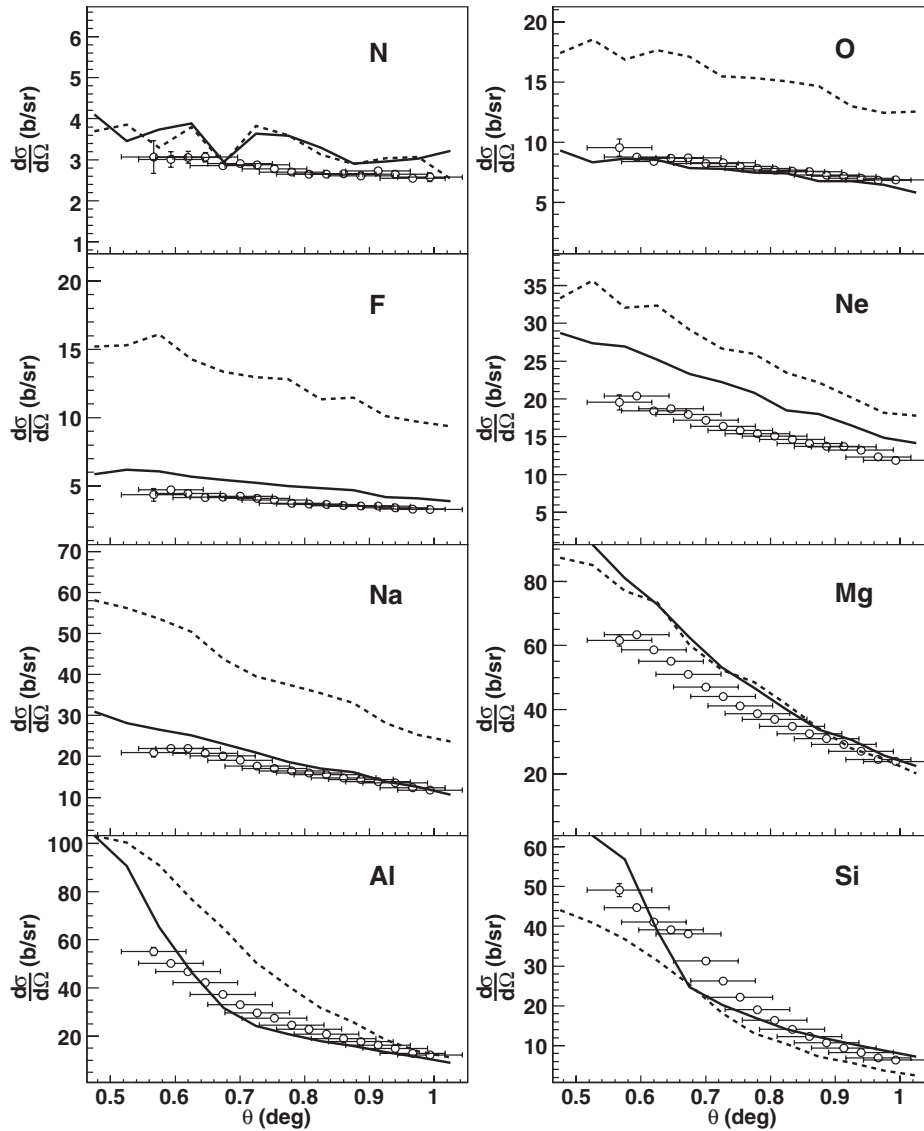


FIG. 4. Angular distribution of recoils in 200 MeV/nucleon  $^{28}\text{Si}+^1\text{H}$  reactions (open points) compared with predictions of DCM (solid curves) and JQMD (dashed curves).

nuclei is quite scarce. Since the 1960s a vast amount of experimental data has been accumulated for the production of radioactive recoils, e.g.,  $^{18}\text{F}$ ,  $^{22}\text{Na}$ , and  $^{24}\text{Na}$  in interactions of medium-energy protons with light nuclei [48]. The unique results of Ref. [8] report on mass, energy, and angular distributions of all products in the  $p+\text{Al}$  reaction at 180 MeV. No similar data exist for other reactions for energies below 500 MeV/nucleon. Figure 5 summarizes the cross sections of recoils detected by SAD in 200- and 300-MeV/nucleon  $^{28}\text{Si}+^1\text{H}$  and  $^{28}\text{Si}+^2\text{H}$  reactions. The results are again confronted with the DCM and JQMD theoretical cross sections filtered through the constraints of the experimental setup. The following remarks can be made.

The predictions from the two models follow in general the experimental distributions. In particular the DCM predictions are impressive with absolute yields within 10% of the measured ones with some exceptions, an overestimation of the Mg production in 200-MeV/nucleon  $^{28}\text{Si}+^2\text{H}$  reactions by 20% and underestimation of Al by 20% in the 300-MeV/nucleon reactions.

The production cross sections of fragments emitted at angles close to  $0^\circ$ , capable of reaching ZAD, show a different behavior (Fig. 6). Although both models predict correctly the increase of the yields with increasing  $Z$  except for  $Z = 14$ , they both overestimate considerably the yields for all  $Z$  at angles close to  $0^\circ$  by factors of 5 to 10. However, a systematic difference is seen between the DCM and JQMD, especially for high  $Z$  values. This will be discussed below.

Figure 7 shows the experimental fragment momentum distributions of  $A/Z = 2$  fragments emitted close to  $0^\circ$  from the 300-MeV/nucleon  $^{28}\text{Si}+^2\text{H}$  reaction compared with the predictions from DCM. It should be noted that the theoretical distributions have been divided by 50 to get the same order of magnitude of the spectra. The model cannot reproduce the shape of the distributions at least for the heavy fragments (Al, Mg, Na, and Ne). If the model overestimates, the low- or high-momentum part is indeterminable because of the large difference in the absolute values. For the lighter fragments it is not that evident due to poor statistics in the theoretical distributions.

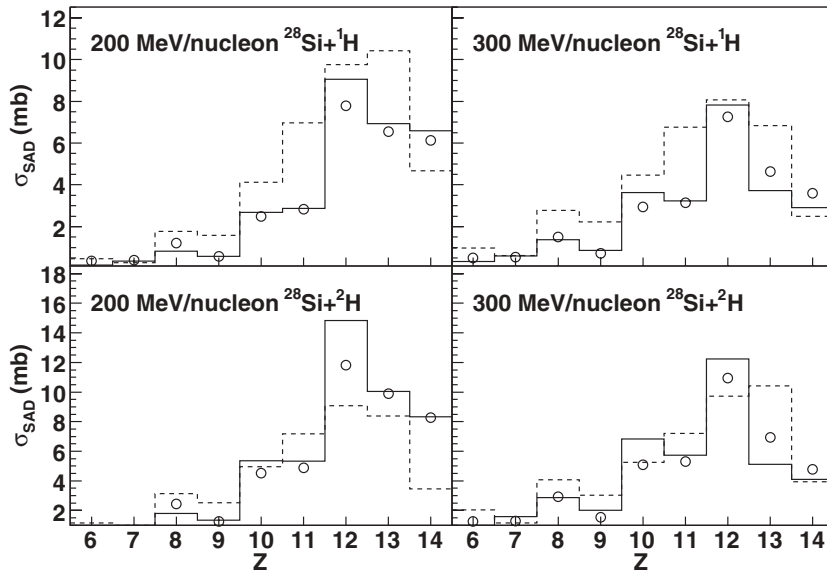


FIG. 5. The cross section for recoils of different charge detected by SAD (open points) compared with the predictions of DCM (solid histograms) and JQMD (dashed histograms).

**B. Recoil-He correlations**

Reactions producing  $Z = 6-13$  recoils within the angular interval  $0.6^\circ-1.1^\circ$ , accompanied by He nuclei, emitted at angles between  $3.9^\circ$  and  $11.7^\circ$  were analyzed through the events with coincidences between SAD and FWD. Figure 8 shows the coincidence yield as a function of the relative azimuthal angle,  $\Delta\phi = \phi_{\text{recoil}} - \phi_{\text{He}}$ , between the recoil and the He fragment. The experimental data are compared with theoretical prescriptions from JQMD and DCM.

The observed distributions are rather broad with centers located around  $\Delta\phi$  values close to  $180^\circ$ . These registered recoils are the heaviest fragments emitted in each collision and normally carry away a substantial part of the total momentum of the decaying system. Momentum conservation in the decaying system prefers that the transverse-momentum components of the two most important fragments are directed back to back. All particles not registered in the setup smear out such an ideal picture. The overall power of the theory to

predict these features could be confirmed only by the shapes of the distributions, whereas the yields are overestimated. The analysis of the rates for the recoil-He correlations registered by SAD and FWD for all reactions is depicted in Fig. 9. Points at  $Z = 13$  and  $14$  are kept to demonstrate the level of the background for this experiment.

A closer look into the experimental data shows that both theories fail to explain correlations of recoils and He in cases of large relative momentum. This is shown in Fig. 10, which demonstrates the dependence of the cross sections for the discussed correlations on the scattering angle of He fragment registered in different rings of the FWD.

The intensity of He-recoil coincidences measured for larger scattering angles of He is considerably higher than that predicted by DCM and JQMD. Again, as in case of low-energy inclusive emission (Fig. 2) a possibility of direct knock-out of  $\alpha$  clusters from the  $^{28}\text{Si}$  nuclei could be discussed with regard to the observed discrepancies between theory and experiment.

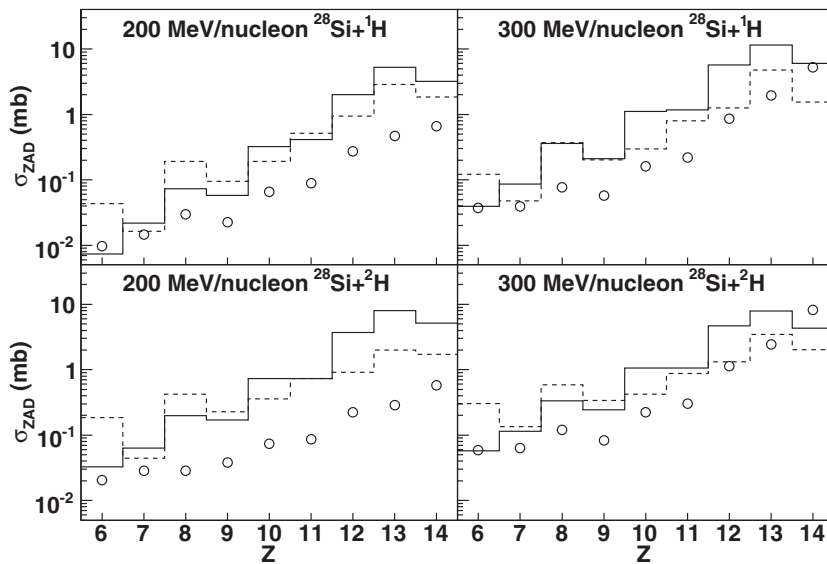


FIG. 6. Measured (open circles) and theoretically predicted DCM (solid histogram) and JQMD (dashed histogram) cross sections for  $^{12}\text{C}$ ,  $^{14}\text{N}$ ,  $^{16}\text{O}$ ,  $^{18}\text{F}$ ,  $^{20}\text{Ne}$ ,  $^{22}\text{Na}$ ,  $^{24}\text{Mg}$ ,  $^{26}\text{Al}$ , and  $^{28}\text{Si}$  reaching ZAD.

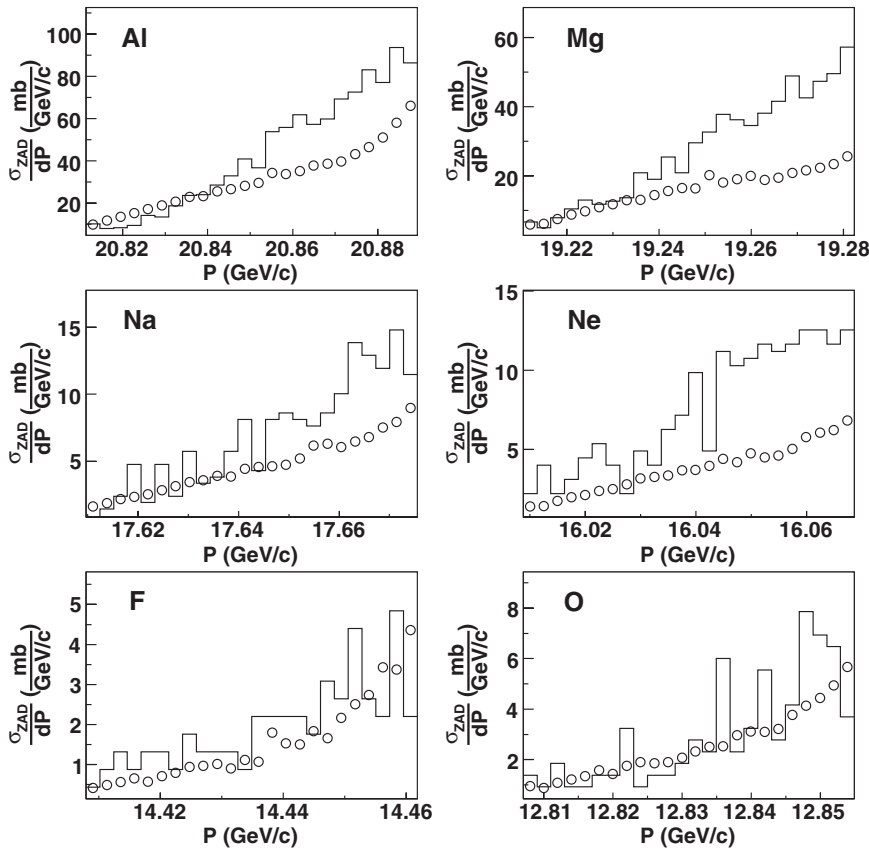


FIG. 7. Momentum distributions of recoils with  $A/Z = 2$  emitted close to  $0^\circ$  in 300 MeV/nucleon  $^{28}\text{Si}+^2\text{H}$  (open points) reactions compared to DCM predictions (histograms). The cross sections for DCM have been divided by 50 to make the comparison of the shapes easier.

### C. Recoil-spectator proton correlations in $^{28}\text{Si}+^2\text{H}$ reactions

The relative cross section for the reaction channel where a recoil in SAD is registered in coincidence with a targetlike spectator, mostly protons, in STD with emission angle between  $60^\circ$  and  $120^\circ$  is shown in Fig. 11. The total cross section for this reaction channel is overestimated in JQMD, whereas it is better reproduced by DCM. The  $Z$  dependence is also better described by DCM although discrepancies still exist. Si and Al are underestimated, whereas O and Ne are overestimated.

The coincidence cross sections show many similarities with the inclusive cross sections in Fig. 5, such as the maximum of the recoil cross sections at  $Z = 12$  and the local minimum for  $Z = 9$ . DCM also shows the same underestimation in producing the heaviest recoils. The increase of the cross section with increasing  $Z$  up to 13 (Al), predicted by JQMD, is observed neither in the data nor in the same model without coincidence. However, it would be dangerous to state that the depicted distributions are tagged by spectator-like protons only. The observed angular distributions of the tagging protons are broad and a large admixture of coincidence events where the registered proton is coming from another source than the target deuteron is possible. This possibly explains the depicted failure of JQMD to describe the experimental data and in any case it calls for additional experimental refinement.

## V. DISCUSSION AND ANALYSIS

The experimental inclusive data on recoil production exhibit a satisfactory overall agreement with both DCM and

JQMD models. This may, however, reflect the ability of both models to describe well the phase space that is available for the products. Both models also predict the  $Z$  dependence quite well of the fragmentation cross section in semiexclusive events with recoil-He correlations. The absolute yields of such events are overestimated by as much as 50–75%.

The two models differ, particularly in their predictions of the yields of the heaviest recoils in favor of DCM, but it should be mentioned that further development of the standard JQMD is already undertaken [44,45]. It is important to note that the situation is quite the opposite when reaction channels with small momentum transfer are addressed. The obvious preference of JQMD, with its built-in ability to describe the dynamical features of reactions, is revealed very distinctly. Figure 6 illustrates also the failure of the DCM to describe the yields of recoils emitted at very small angles due to the dynamical effects that that model totally ignores. Although not influencing the predictive power of the DCM, this reflects the limitation of the “frozen mean-field” approximation of that model. On the contrary, the ability of JQMD to describe the same data better than DCM could be explained by its ability, at least qualitatively, to describe collective “bounce-off” attributed to the dynamics of the reaction.

The ability of any of these theories to prescribe the reaction channels generating He seems questionable. An overall agreement between theory and experiment on inclusive production of He is observed only for the DCM and only if the deep sub-barrier component is not considered. JQMD fails to prescribe the slopes of the He spectra and the QMD approach is known to meet principle difficulties in



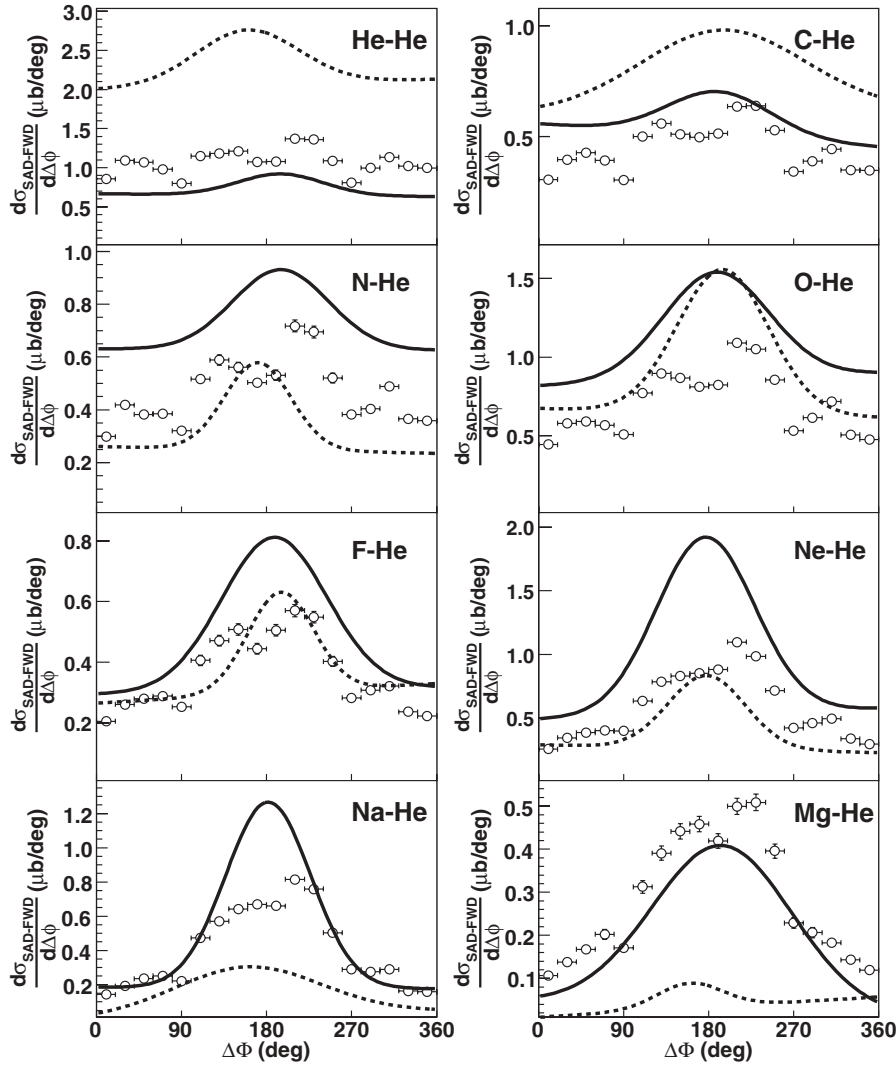


FIG. 8. Azimuthal correlations between recoils and He fragments registered by SAD and FWD. Experimental results on 300 MeV/nucleon  $^{28}\text{Si}+^2\text{H}$  reactions (open points) are compared with predictions from DCM (solid lines) and JQMD (dashed lines).

describing  $\alpha$  particles [47] due to their specific properties. The improvements of JQMD discussed in Sec. IV A could improve the inclusive angular distribution of He but we believe that these improvements will not alter our basic conclusions.

The experiment revealed two specific features of the reactions that neither DCM nor JQMD can handle. Both features are of greatest importance for the further development of the models and they could probably lead to substantial

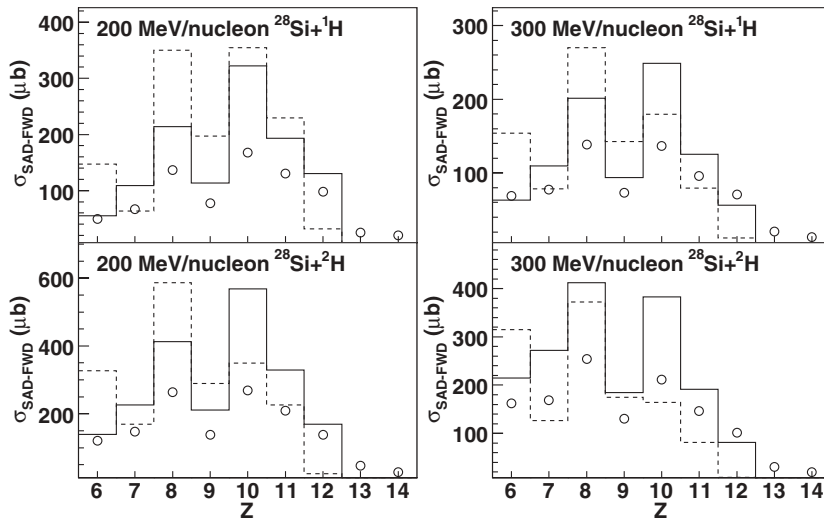


FIG. 9. Charge dependence of the cross section for correlations between recoils measured by SAD and He fragments registered by FWD (open points) compared with predictions of DCM (solid histograms) and JQMD (dashed histograms).

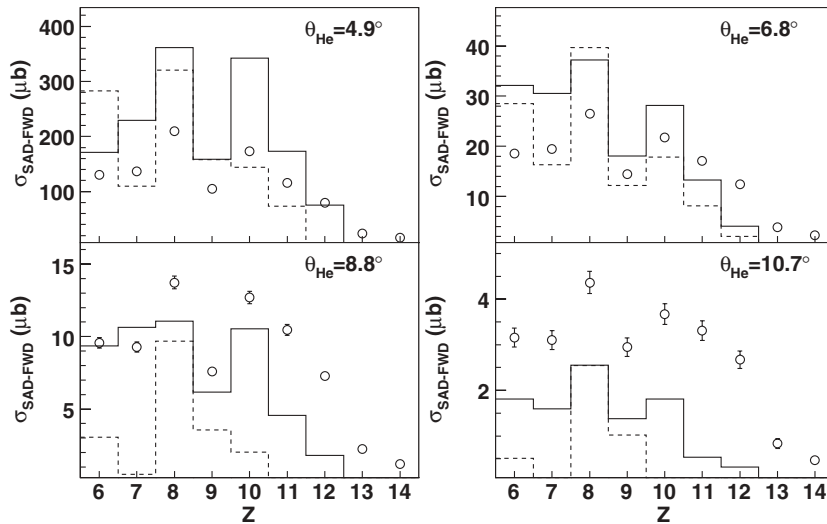


FIG. 10. Recoil-He correlation cross sections for different charge of the recoil in 300-MeV/nucleon  $^{28}\text{Si}+^2\text{H}$  reactions. The emission angle ranges from  $4.9^\circ$  (upper left) to  $10.7^\circ$  (lower right). Data (open points) and predictions by DCM (solid lines) and JQMD (dashed lines).

improvement of their prediction power. First, although the total cross section for the recoil-He correlation is described well by both models the cross section for such correlations at larger scattering angle (relative momentum) is much larger in the experiment. There exists a number of predictions of preformed  $\alpha$  clustering in light nuclei [49]. It seems obvious that future modifications of models like DCM and JQMD should address this problem specifically for light nuclei. Second, a considerable excess of He products within the acceptance of SAD has been observed for which DCM seems to have no definite explanation. SAD has an extremely low detection threshold of 100 keV for He fragments in their production system. These He nuclei could not be measured in conventional experiments. A reasonable explanation is again to be found in  $\alpha$  clustering in  $^{28}\text{Si}$ .

The apparent difference between the cross sections for production of recoils from the data of Figs. 5 and 6 and the results reported in Ref. [8] is misleading due to the following reasons. First, no direct comparison is possible for the data of this article to that previously reported for the 180-MeV  $p+\text{Al}$

reaction summarized in Ref. [8], our article focused on charge distributions, whereas that of the authors of Ref. [8] focused on mass distributions. To link the two sets of data, one needs to know the isotopic distributions of the reaction products, which, in fact, turn out to be strongly model dependent. Second, one should be aware that, due to the experimental setup, the recoil charge distributions demonstrated in Figs. 5 and 6 refer to recoil yields integrated within the angular acceptance of SAD or ZAD and essentially differ from the total recoil cross sections, especially in case of lighter recoils.

The similarity in the differential cross sections in Figs. 3 and 4 for all recoils except Si might indicate that saturation of the fragmentation cross sections has been reached at 200 MeV/nucleon. However, data in Fig. 6 show that this statement is not valid for recoils emitted at very small angles. As mentioned above, our experimental setup covered only a part of the available phase space and therefore, direct measurements of the total cross sections are needed before definite conclusions on the energy threshold for limiting fragmentation of Si can be made.

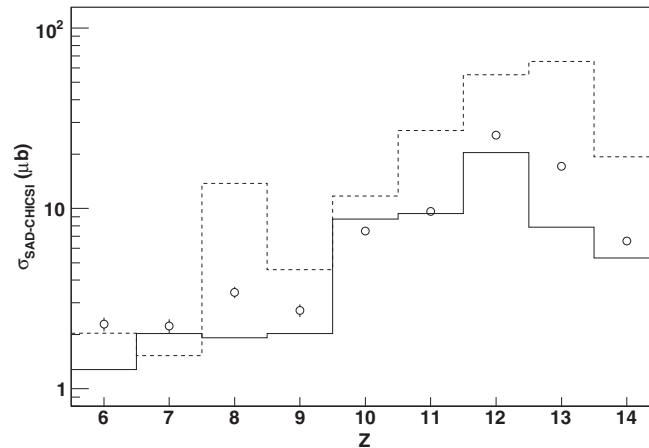


FIG. 11. Charge dependence of the cross section in 300-MeV/nucleon  $^{28}\text{Si}+^2\text{H}$  reactions for a recoil in SAD in coincidence with a low-energy proton in STD. Notations are the same as described in the caption to Fig. 10.

## VI. SUMMARY

We measured the relative production cross sections of recoils from 200- and 300-MeV/nucleon proton and deuteron-induced reactions with  $^{28}\text{Si}$  nuclei. The data, obtained in the inverse kinematics scheme, were compared with predictions from the hybrid DCM and JQMD models.

It was found that in general both models describe reasonably well the overall charge and angular distributions of the fragmentation cross sections but the absolute yields differ by as much as 50–75%. The number of recoils emitted at very small angles is described reasonably well only within the frame of the JQMD model, which we attributed to the “bounce-off” of the source of recoils, which cannot be described by the DCM. These experimental observations call for improvements of the models before using them for SEEs predictions.

Two features of the studied reactions are not described at all by the models: first, the growing excess of the experimental cross sections for the recoil-He correlation over standard theory with increasing scattering angle between the recoil and He. This may be linked to the knock-out process of He from

$^{28}\text{Si}$ , usually explained in terms of preformed  $\alpha$  clustering. Second, we observe a large excess of low-energy He fragments that could also be explained qualitatively by  $\alpha$  clustering in  $^{28}\text{Si}$  nuclei.

These observations call for additional experimental and theoretical study of fragmenting nuclear systems with large initial admixture of  $\alpha$  clusters that in turn could lead to a considerable improvement of the reaction models of primary importance for the SEEs application.

## ACKNOWLEDGMENTS

We are grateful for all help that the staff of TSL provided and especially for the extraordinary efforts made by the TSL accelerator team, headed by Dag Reistad. This project has been funded by the US Party of the International Science and Technology Center (ISTC) [50], for which we are deeply grateful. Our thanks go also to the FOI, Sweden, providing funds to support stays of the international team at TSL.

- 
- [1] H. H. K. Tang, IBM J. Res. Dev. **40**(1), 91 (1996).  
 [2] H. H. K. Tang and N. Olsson, MRS Bull. **28**(2) (2003).  
 [3] V. D. Toneev and K. K. Gudima, Nucl. Phys. **A400**, 173 (1983).  
 [4] K. K. Gudima, S. G. Mashnik, and V. D. Toneev, Nucl. Phys. **A401**, 329 (1983).  
 [5] K. Niita, S. Chiba, T. Maruyama, T. Maruyama, H. Takada, T. Fukahori, Y. Nakahara, and A. Iwamoto, Phys. Rev. C **52**, 2620 (1995).  
 [6] P. Goldhagen, MRS Bull. **28**, 131 (2003).  
 [7] F. E. Bertrand and R. W. Peelle, Phys. Rev. C **8**, 1045 (1973).  
 [8] K. Kwiatkowski, S. H. Zhou, T. E. Ward, V. E. Viola, H. Breuer, G. J. Mathews, A. Gökmen, and A. C. Mignerey, Phys. Rev. Lett. **50**, 1648 (1983).  
 [9] H. Machner, D. G. Aschman, K. Baruth-Ram, J. Carter, A. A. Cowley, F. Goldenbaum, B. M. Nangu, J. V. Pilcher, E. Sideras-Haddad, J. P. F. Sellschop *et al.*, Phys. Rev. C **73**, 044606 (2006).  
 [10] L. W. Woo, K. Kwiatkowski, W. G. Wilson, V. E. Viola, H. Breuer, and G. J. Mathews, Phys. Rev. C **47**, 267 (1993).  
 [11] M. B. Chadwick, S. Chiba, K. Niita, T. Maruyama, and A. Iwamoto, Phys. Rev. C **52**, 2800 (1995).  
 [12] S. Chiba, M. B. Chadwick, K. Niita, T. Maruyama, T. Maruyama, and A. Iwamoto, Phys. Rev. C **53**, 1824 (1996).  
 [13] H. H. K. Tang, G. R. Srinivasan, and N. Azziz, Phys. Rev. C **42**, 1598 (1990).  
 [14] J. Cugnon and J. Vandermeulen, Ann. Phys. (Paris) **17**, 49 (1989).  
 [15] J. Cugnon and P. Henrotte, Eur. Phys. J. A **16**, 393 (2003).  
 [16] Y. Murin *et al.*, *STORI 05, Schriften des Forschungszentrums Jülich. Reihe Materie und Material/Matter and Materials 30*, edited by David Chiladze, Andro Kacharava, Hans Ströher (Forschungszentrum Jülich, Zentralbibliothek, Verlag, Jülich, 2005), p. 153.  
 [17] J. Aichelin, C. Bargholtz, J. Blomgren, A. Budzanowski, M. Chubarov, B. Czech, C. Ekström, L. Gerén, B. Jakobsson, A. Kolozhvari *et al.*, in *Proceedings of International Conference on Nuclear Data for Science and Technology*, Santa Fe, NM, September 26–October 1, 2004, AIP Conf. Proc. No. 769, edited by Robert C. Haight, Mark B. Chadwick, Toshihiko Kawano, and Patrick Talou (AIP, New York, 2005), p. 1624.  
 [18] C. C. Foster, P. M. O’Neill, and C. K. Kouba, IEEE Trans. Nucl. Sci. **53**, 3494 (2006).  
 [19] Y. Murin, Y. Babain, M. Chubarov, Y. Tuboltsev, V. Pljushev, M. Zubkov, P. Nomokonov, A. Voronin, M. Merkin, V. Kondratiev *et al.*, Nucl. Instrum. Methods A **578**, 385 (2007).  
 [20] A. Budzanowski, B. Czech, A. Siwek, I. Skwirczynska, and P. Staszal, Nucl. Instrum. Methods A **482**, 528 (2002).  
 [21] L. Westerberg, V. Avdeichikov, L. Carlén, P. Golubev, B. Jakobsson, C. Rouki, A. Siwek, E. J. van Veldhuizen, and H. J. Whitlow, Nucl. Instrum. Methods A **500**, 84 (2003).  
 [22] P. Golubev, V. Avdeichikov, L. Carlén, B. Jakobsson, A. Siwek, E. J. van Veldhuizen, L. Westerberg, and H. J. Whitlow, Nucl. Instrum. Methods A **500**, 96 (2003).  
 [23] L. Carlén, G. Førre, P. Golubev, B. Jakobsson, A. Kolozhvari, P. Marciniowski, A. Siwek, E. J. van Veldhuizen, L. Westerberg, H. J. Whitlow *et al.*, Nucl. Instrum. Methods A **516**, 327 (2004).  
 [24] C. Bargholtz, K. Lindh, D. Protic, N. Ruus, P.-E. Tegnér, P. T. Engblom, and K. W. Rolander, Nucl. Instrum. Methods A **390**, 160 (1997).  
 [25] A. Ringbom, G. Tibell, R. Zorro, J. Blomgren, H. Condé, K. Elmgren, S. Hultqvist, J. Nilsson, N. Olsson, C. Fahlander *et al.*, Nucl. Instrum. Methods A **373**, 57 (1996).  
 [26] R. Serber, Phys. Rev. **72**, 1114 (1947).  
 [27] G. D. Harp and J. M. Miller, Phys. Rev. C **3**, 1847 (1971).  
 [28] J. J. Griffin, Phys. Lett. **B24**, 5 (1967).  
 [29] M. Blann and M. B. Chadwick, Phys. Rev. C **57**, 233 (1998).  
 [30] H. Feshback, A. Kerman, and S. Koonin, Ann. Phys. (NY) **125**, 429 (1980).  
 [31] G. F. Bertch and S. Das Gupta, Phys. Rep. **160**, 189 (1988), and references therein.  
 [32] J. Aichelin, Phys. Rep. **202**, 233 (1991), and references therein.  
 [33] H. Feldmeier, Nucl. Phys. **A515**, 147 (1990).

- [34] A. Ono, H. Horiuchi, T. Maruyama, and A. Ohnishi, *Prog. Theor. Phys.* **87**, 1185 (1992).
- [35] S. G. Mashnik, K. K. Gudima, A. J. Sierk, M. I. Baznat, and N. V. Mokhov, Los Alamos National Laboratory Report LA-UR-05-7321.
- [36] S. Furihata, *Nucl. Instrum. Methods B* **171**, 251 (2000).
- [37] E. Fermi, *Prog. Theor. Phys.* **5**, 570 (1950).
- [38] V. D. Toneev, N. S. Amelin, K. K. Gudima, and S. Y. Sivoklov, *Nucl. Phys.* **A519**, 493 (1990).
- [39] N. S. Amelin, K. K. Gudima, and V. D. Toneev, *Sov. J. Nucl. Phys.* **50**, 172 (1990), and references therein.
- [40] R. J. Charity, *Nucl. Phys.* **A483**, 371 (1988).
- [41] S. Chiba, O. Iwamoto, T. Fukahori, K. Niita, T. Maruyama, T. Maruyama, and A. Iwamoto, *Phys. Rev. C* **54**, 285 (1996).
- [42] T. Maruyama, K. Niita, and A. Iwamoto, *Phys. Rev. C* **53**, 297 (1996).
- [43] Y. Watanabe, A. Kodama, Y. Tukamoto, and H. Nakashima, in *Proceedings of International Conference on Nuclear Data for Science and Technology*, Santa Fe, NM, September 26–October 1, 2004, AIP Conf. Proc. No. 769, edited by Robert C. Haight, Mark B. Chadwick, Toshihiko Kawano, and Patrick Talou (AIP, New York, 2005), p. 1646.
- [44] Y. Watanabe and D. N. Kadrev, *Radiation Protection Dosimetry*, **126**, 1 (2007).
- [45] H. Iwase, K. Niita, and T. Nakamura, *J. Nucl. Sci. Technol.* **39**, 1142 (2002).
- [46] U. Tippawan, S. Pomp, A. Ataç, B. Bergenwall, J. Blomgren, S. Dangtip, A. Hildebrand, C. Johansson, J. Klug, P. Mermod *et al.*, *Phys. Rev. C* **69**, 064609 (2004).
- [47] A. Ono (private communication).
- [48] R. G. Korteling and A. A. Caretto, *Phys. Rev. C* **1**, 193 (1970).
- [49] J. A. Maruhn, M. Kimura, S. Schramm, P.-G. Reinhard, H. Horiuchi, and A. Tohsaki, *Phys. Rev. C* **74**, 044311 (2006).
- [50] [Http://www.istc.ru](http://www.istc.ru).